Implementation of a graded-index medium by use of subwavelength structures with graded fill factor

Uriel Levy, Maziar Nezhad, Hyo-Chang Kim, Chia-Ho Tsai, Lin Pang, and Yeshaiahu Fainman

Department of Electrical and Computer Engineering, University of California, San Diego, 9500 Gilman Drive, La Jolla, California 92093-0407

Received June 8, 2004; revised manuscript received September 29, 2004; accepted October 27, 2004

We present a novel configuration for the implementation of subwavelength-based graded-index devices. The proposed concept is based on the etching of one-dimensional subwavelength gratings into a high-index slab waveguide to achieve the desired effective index distribution. A graded-index profile can be achieved by gradually modifying the duty ratio of the grating along the horizontal axis, while the beam is confined in the vertical direction by the slab waveguide. On the basis of this concept, novel graded-index lenses and waveguides are both proposed and characterized numerically by use of finite-difference time-domain and finite-element analysis. The proposed devices can be used for guiding, imaging, optical signal processing, mode matching, coupling, and other applications while offering the intrinsic advantages of on-chip integration such as miniaturization, eliminating the need to align each component separately, and compatibility with standard microfabrication techniques for manufacturability.

OCIS codes: 050.2770, 130.3120, 350.3950.

1. INTRODUCTION

Over the past decade, subwavelength optical structures (sometimes called nanostructures when the feature size is of the order of hundreds of nanometers or below) have been widely investigated and engineered in free-space configurations to create unique anisotropic, dispersive, and nonlinear optical properties.[1–7] These structures, commonly composed of one-dimensional (1-D) subwavelength periodic or aperiodic geometries, are characterized by an effective refractive index that is usually different for the TE and the TM polarization states of the optical fields. Such subwavelength-based optical anisotropic materials have been used for realization of polarization components such as birefringent wave plates and polarization converters.[8–10] Artificial modification of the refractive index has been also used for fabrication of diffractive optical elements.[11–15]

Design and analysis of subwavelength structures can be performed with the effective-medium theory approximation,[16] provided that the structures are much smaller than the optical wavelength in the material. For higher accuracy or when the simplifying assumptions are not valid, more accurate but computationally complex approaches can be used, including rigorous coupled-wave analysis (RCWA),[17] the finite-difference time-domain (FDTD) method,[18] the boundary integral method,[19] or the finite-element method.[20]

Typically, subwavelength-based components can be fabricated with an aspect ratio of 1:1–10:1 (i.e., the ratio between the thickness and the width of the structure). As a result, for free-space applications the interaction length between the optical field and the engineered structure is limited to a few optical wavelengths only. Although such short interaction lengths are sufficient for the design and implementation of subwavelength-based diffractive-type elements,[11–15] so far it has prevented use of these structures in other important applications such as dispersion management and refractive beam manipulation and shaping. A concrete example for components that require an interaction length much larger than a single optical wavelength are graded-index-based optical components and devices. Such a graded-index medium is widely used both in free space as well as in guided-wave configurations. Two commonly known examples are the graded-index lens used for focusing, collimation, and mode matching and the graded-index waveguide that provides a significantly reduced value of dispersion compared with a standard multimode waveguide, also allowing easier coupling compared with a single-mode waveguide (typically due to a larger mode size). Both types of device can also be utilized for optical transformations such as the fractional Fourier transform.[21]

The issue of limited interaction length, however, does not apply to a slab waveguide configuration with engineered subwavelength structures to modulate the effective index of refraction. So far, such a configuration has been primarily used for realization of two-dimensional (2-D) photonic crystals, where the slab is used for beam confinement in the vertical axis.[22–24] With such a configuration, the beam is propagating along the slab; thus the interaction length is practically limited only by the field size of the fabrication tool. Typically, photonic crystals are designed and implemented around their bandgap region, i.e., light cannot propagate through the photonic crystal structure. Light propagation is controlled by introducing a defect line in the structure.[22] Therefore the light is guided within the defect whereas the photonic crystal structure is used as an efficient cladding layer in

the horizontal direction. The confinement along the vertical direction is achieved through larger effective index difference between the layers. It should be noted that there are some examples in which the photonic crystal is designed to operate slightly below the bandgap, mainly to achieve superprism[25] and supercollimation effects.[26,27]

In this paper we introduce a new type of graded-index device, implemented by etching 1-D subwavelength structures into a slab waveguide made of high-index material (e.g., semiconductor, dielectric, or composite). The proposed structure has a fixed periodicity in the x direction (see Fig. 1), with the duty ratio varied to control the local effective refractive index. Vertical confinement in the y direction is provided by the effective high refractive index of the slab layer, similar to a slab photonic crystal configuration. The effective index profile varies gradually along the horizontal axis. This is in contrast to a previous approach, where the graded-index profile was implemented in the vertical axis by growing a multilayer structure with gradually varying index.[28] A large interaction length is now achieved since the light is propagating in the z direction along the plane of the patterned slab (see Fig. 1) rather than in the free-space configurations with light propagating in a direction perpendicular to the plane of the slab. To some extent, the proposed structures resemble those used for guided-mode resonance filters,[29,30] although the latter are usually implemented with a slightly larger period-to-wavelength ratio (since a diffraction order is desired) and with a constant duty ratio. Also, the propagation of the guided mode is perpendicular to the grating lines (i.e., along the x axis).

By use of our proposed approach, 2-D (x, z) Fourier optics concepts can now be applied for light propagating in the z direction. Specifically, we introduce and analyze specific design examples of devices for the focusing and guiding of light. This approach can be used for guiding, imaging, mode matching, and optical signal processing while offering an intrinsic advantage of on-chip integration. The need to align discrete components relative to each other is eliminated, exploiting a high level of integration made possible by existing and developing nanofabrication methods for cost-effective manufacturing.

In Section 2 we describe the analysis and design concepts of nanostructure-based graded-index media. In Section 3 we advance our analysis and design of some specific device examples for focusing and guiding optical fields. Technological considerations are presented in Section 4. Conclusions and discussions are provided in Section 5.

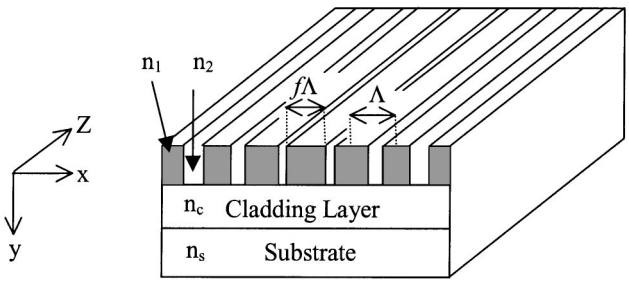

Fig. 1. Proposed graded-index structure. The beam propagates along the z axis, and the duty ratio is varied along the horizontal axis. Vertical confinement is achieved by the slab waveguide.

2. DESIGN OF GRADED-INDEX MEDIA BASED ON SUBWAVELENGTH STRUCTURES

Our design is based on engineering the effective index within a slab waveguide by etching subwavelength structures into the slab (see Fig. 1). For simplicity, we assume that the beam is well confined within the slab layer, allowing us to use 2-D analysis. This assumption will be further discussed below.

We exploit the modulation of the local effective index by modifying the duty ratio of the etched structure. Using the second-order effective-medium theory,[16] we approximate the effective index by

$$[n_{\mathrm{TE}}^{(2)}]^2 = [n_{\mathrm{TE}}^{(0)}]^2 + \frac{1}{3}\left[\frac{\Lambda}{\lambda}\pi f(1-f)({n_1}^2 - {n_2}^2)\right]^2, \tag{1a}$$

$$[n_{\mathrm{TM}}^{(2)}]^2 = [n_{\mathrm{TM}}^{(0)}]^2 + \frac{1}{3}\left\{\frac{\Lambda}{\lambda}\pi f(1-f)\left(\frac{1}{{n_1}^2} - \frac{1}{{n_2}^2}\right) n_{\mathrm{TE}}^{(0)} \times [n_{\mathrm{TM}}^{(0)}]^3\right\}^2 \tag{1b}$$

for TE (i.e., $\mathbf{E} = E\hat{y}$) and TM (i.e., $\mathbf{H} = H\hat{y}$) states of polarization, respectively; Λ is the period of the structure, λ is the optical wavelength in vacuum, f is the duty ratio, $n_{1,2}$ are the two refractive indices composing the structure, and

$$[n_{\mathrm{TE}}^{(0)}]^2 = f{n_1}^2 + (1-f){n_2}^2,$$

$$[n_{\mathrm{TM}}^{(0)}]^2 = \frac{(n_1 n_2)^2}{f{n_2}^2 + (1-f){n_1}^2}.$$

Equations (1) are an approximate solution for the effective index, since they contain only the first two terms in the Taylor expansion of a tangent function.[16] Nevertheless, they can be assumed to provide reasonable accuracy as long as $\Lambda < \lambda/n$, where $n = \max[n_1, n_2]$ (Ref. 1) and the grating thickness is not too small [e.g., larger than $\lambda/3$ (Ref. 31)]. In general, we can achieve almost any desired index profile for various purposes. One of the commonly used descriptions for a refractive-index profile is a polynomial function given by

$${n_0}^2(x) = {n_0}^2(1 - \alpha x^p), \tag{2}$$

where α and p are constants for a special design. For example, when $p = 1$ a linear index profile is obtained. Such a profile would be appealing for applications involving tilting or bending of light. In this paper our main focus is aimed toward the design and the investigation of devices for focusing and guiding of light. Thus we focus on the investigation of subwavelength-based devices with a quadratic index profile ($p = 2$). Such an index profile represents a periodic system where the beam shape and curvature repeats itself at intervals proportional to $1/\sqrt{\alpha}$.

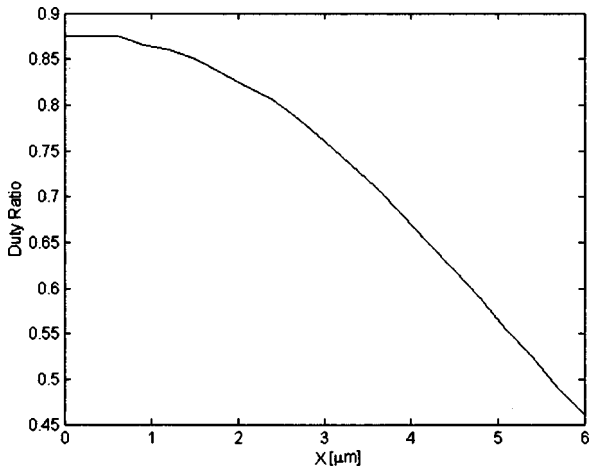

Fig. 2. Duty ratio versus lateral distance from the optical axis for TE polarization: $n_0 = 3.2$, $\alpha = 0.01$ ($1/\mu m^2$), $\lambda = 1.55\,\mu m$, $\Lambda = 0.3\,\mu m$, $n_1 = 3.37$, $n_2 = 1$.

This index profile is widely used to implement graded-index waveguides, fibers, and lenses. Focusing and guiding of light can also be achieved by generating a periodic sawtooth effective index profile. For such a case, the structure is expected to act as a Fresnel waveguide.[32]

Next we assume $p = 2$ in Eq. (2), and from a comparison with Eqs. (1) we find the desired duty ratio as a function of the lateral coordinate. A typical solution for f versus the deviation from the optical axis for the TE-polarized field is shown in Fig. 2. In our simulations we assume the following parameters: $\lambda = 1.55\,\mu m$, $\Lambda = 0.3\,\mu m$, $n_1 = 3.37$ (GaAs), and $n_2 = 1$ (air). We obtained the result in Fig. 2 by using Eq. (1a), but similar results were also obtained with 2-D FDTD and RCWA simulations. For the RCWA simulation we assumed that the refractive-index profile varies slowly on the wavelength scale so that we could calculate the local properties by assuming an infinitely periodic structure, neglecting the influence of the duty ratio variations on the local effective index. As expected, f is smoothly reduced as the distance from the optical axis increases, reducing the effective refractive index. It should be noted that the obtained profile would be only a staircase approximation of the desired continuous index profile, leading to the introduction of a quantization error. To estimate the quantization error, we assume a relatively slow gradient for the index along the x axis on distances comparable to Λ. For such a case, the effective refractive index can be approximated by

$$n(x) = n_0\left(1 - \frac{1}{2}\alpha x^2\right). \tag{3}$$

The maximal index deviation from the desired continuous profile is

$$\max\left(\frac{\Delta n}{n}\right) = \max\left(\frac{1}{n}\frac{dn}{dx}\Delta x\right) \approx \frac{1}{2}\alpha\Lambda\omega, \tag{4}$$

where ω is the beam half-width and $\Delta x = \Lambda/2$ is assumed. Equation (4) was obtained by assuming a continuous control over the duty ratio, such that the error source results only from the sampling (owing to the finite period size). If the control over the duty ratio is also limited in accuracy, this additional error source needs to be taken into consideration, as discussed in Section 4. Considering typical values of $\Lambda = 0.4\,\mu m$ (the period should be smaller than λ/n to avoid internal diffraction orders) and a beam half-width of 5 μm, it is a good practice to keep α no larger than 0.01–0.02 ($1/\mu m^2$). For these values, the deviation from the desired profile is of the order of 1%, thus having a negligible effect on the beam propagation. For such slow variations of the refractive-index profile, the system can be assumed to be paraxial, and the beam propagation can be analyzed with the $ABCD$ law:

$$q_{out} = \frac{Aq_{in} + B}{Cq_{in} + D}, \tag{5}$$

where the beam parameter q is given by

$$\frac{1}{q} = \frac{1}{R(z)} + j\frac{\lambda}{\pi\omega^2(z)}. \tag{6}$$

Here $\omega(z)$ and $R(z)$ are the beam transverse half-width and the wave-front curvature radius, respectively. The origin of coordinate z is measured from the beam waist, defined as the transverse plane where the beam half-width $\omega_0(z)$ reaches its minimal value and its wave-front radius of curvature tends to infinity (i.e., plane wave front). The matrix describing the propagation of a Gaussian beam within the quadratic index media is given by[33]

$$\begin{bmatrix} A & B \\ C & D \end{bmatrix} = \begin{bmatrix} \cos(rd) & \dfrac{\sin(rd)}{r} \\ -r\sin(rd) & \cos(rd) \end{bmatrix}, \tag{7}$$

where the parameter r is related to the parabolic parameter α by $r = \sqrt{\alpha}$ and d is the length of the component along the z axis. Such a matrix describes a periodic system with a period of $rd = 2\pi m$, $m = 0, 1, 2, \ldots$; i.e., the beam width and the wave-front radius of curvature will repeat itself at distances of $z = (2\pi m)/r$.

Before presenting some specific examples, we first discuss the effect of the finite thickness of the structure. In the following, we assume a 1-μm-thick GaAs slab ($n = 3.37$) on top of a thick aluminum oxide (Al_xO_y, $n_c = 1.5$). The surrounding is assumed to be air ($n = 1$). Clearly, the effective index within the slab will be smaller than that of bulk GaAs since a portion of the slab mode exceeds the slab dimensions and interacts with the cladding layers. For a nonpatterned GaAs layer, the effective index of our asymmetric slab is $n_{es} = 3.28$ for TE and $n_{es} = 3.30$ for TM.[34] The overall effective index resulting from patterning the GaAs layer with the subwavelength structures can now be calculated with Eqs. (1) by replacing n_1 with n_{es} (approach 1). Alternatively, we can use Eqs. (1) to find a local effective index value for the structured slab layer and use this value to calculate the overall effective index of the mode within the slab (approach 2). Figure 3 shows the calculated effective index within the slab as a function of the duty ratio by use of

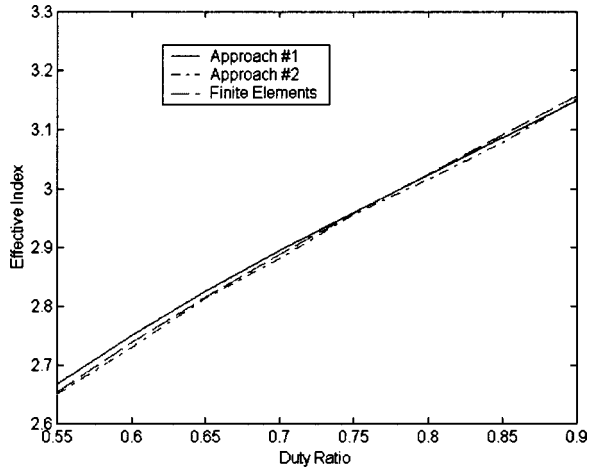

Fig. 3. Effective index of the patterned slab versus duty ratio for TE polarization: $\Lambda = 0.3\,\mu$m, $n_1 = 3.37$, $n_2 = 1$. Slab thickness is 1 μm.

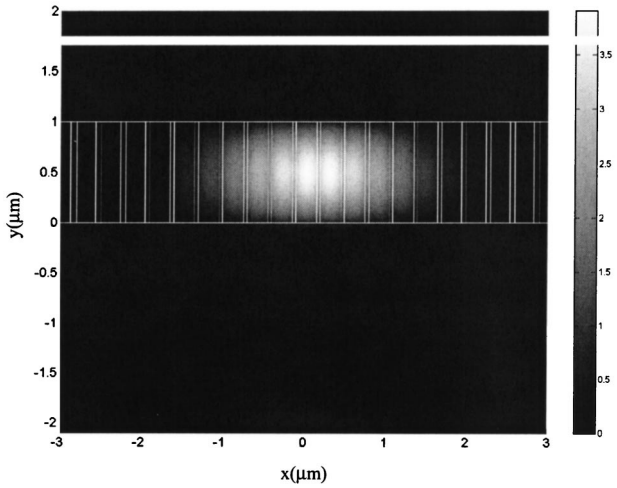

Fig. 4. Typical beam cross section traveling along subwavelength-based graded-index media. The structure is composed of a 1-μm GaAs slab layer on top of an aluminum oxide cladding layer. The GaAs layer is patterned with a structure having a period of $\Lambda = 0.3\,\mu$m. The duty ratio is calculated according to Eq. (1a) to achieve an effective index profile with $n_0 = 3.1$ and $\alpha = 0.01$ ($1/\mu$m^2).

these two approaches, indicating that the two approaches reveal almost identical results. For validation purposes, we also display the results obtained by a finite-element simulation using COMSOL Inc. commercial FEMLAB 3 software. It is evident that all three approaches are in good agreement. For qualitative demonstration purposes, a typical mode structure within a graded-index nanostructured slab with parameters $n_0 = 3.1$, $\alpha = 0.01$ ($1/\mu$m^2) is depicted in Fig. 4.

As mentioned above, our approach is based on free-space analysis for the propagation in the horizontal-axis direction, while the beam is confined by a slab-guiding mode in the vertical-axis direction. To maintain the beam confinement and avoid radiation loss, the subwavelength structured-based slab must support at least a single guiding mode. Thus we need to verify that the effective index of the subwavelength structure is above the critical index to achieve guiding properties. For the proposed configuration, the critical index of the slab is 1.534 for TM and 1.54 for TE polarization; from using Eqs. (1) we find that the minimal duty ratio allowing guidance in the nanostructured slab is 0.12 for TE and 0.55 for TM polarization.

An additional concern is the effect of having several modes along the vertical axis. In fact, a relatively thin slab layer (e.g., 0.3 μm) will ensure a single vertical mode. However, using such a thin layer is sometimes undesirable, mainly because of the low efficiency of light coupling from an optical fiber into the slab waveguide. Increasing the thickness of the slab layer offers a prominent advantage in terms of light-coupling efficiency. Obviously, this in turn will increase the number of vertical modes that will be guided by the slab. Since the effective index for each mode will be different, one might expect slightly different values of α for each mode, leading to a difference in the periodic length of our graded-index structure for each of these modes. To estimate the propagation of higher-order slab modes within the graded-index structure, we consider a specific example of a 0.65-μm-thick GaAs layer on top of aluminum oxide. For simplicity, we evaluate and discuss only TE modes. This slab structure can support two modes as long as the effective index of the subwavelength pattern is kept in the range of 2.2–3.15, in turn corresponding to a duty ratio varying in the range of 0.32–0.84 [see Eq. (1a)].

To evaluate the effective index profile obtained for the higher modes, we optimize a graded-index structure to provide a quadratic profile for the fundamental mode and calculate the resulting effective index profile for the second mode. The effective indices of the nonpatterned slab for these two modes are $n_{es} = 3.19$ and 2.61. Our desired quadratic index profile for the fundamental mode is represented by $n_0 = 2.96$ and $\alpha = 0.01$ ($1/\mu$m^2). The required duty ratio profile used to implement these values is calculated from a comparison of Eq. (1a) with Eq. (2) while using $n_{es} = 3.19$ in Eq. (1a). On the basis of the obtained duty ratio profile, we can now estimate the ob-

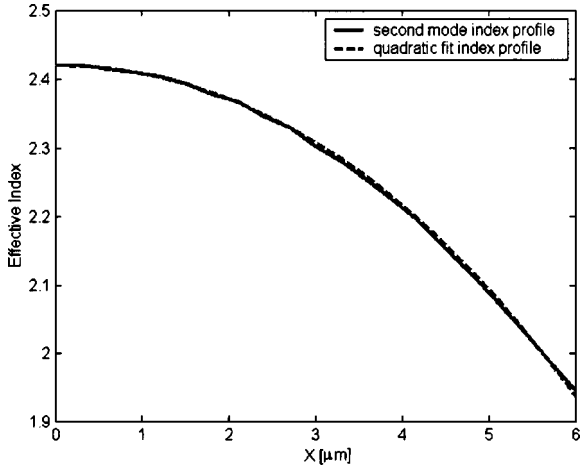

Fig. 5. Effective index of the second slab mode for a quadratic profile optimized for the first mode. Solid curve, obtained index profile; dashed curve, fitting to a modified quadratic profile with $n_0' = 2.42$, $\alpha' = 0.01$ ($1/\mu$m^2). Slab thickness is 0.65 μm, with an effective index of 3.19 and 2.61 for the two modes, respectively.

tained overall effective index for the second mode, using $n_{es} = 2.61$ in Eq. (1a). The resulting index profile for the second mode is shown in Fig. 5 (solid curve). By fitting this profile to a modified quadratic profile $[n' = n_0'(1 - \alpha' x^2)]$, we obtained $n_0' = 2.42$, $\alpha' = 0.01$ $(1/\mu m^2)$. The profile described by these fitting parameters is shown by the dashed curve in Fig. 5, indicating a close match with the actual profile. If we further increase the slab thickness, additional supported modes will need to be taken into consideration. For example, by choosing a slab thickness of 1 μm (which is already challenging in terms of the required aspect ratio values), the slab can support three additional modes, with effective indices of 3.04, 2.59, and 1.90, respectively. The index profile for these modes (obtained by curve fitting) is given by $n_0' = 2.87, 2.45, 1.81$ and $\alpha' = 0.01, 0.01, 0.009$ $(1/\mu m^2)$, respectively. Considering the practical configurations, we can now derive two major conclusions: (i) although a graded-index device with a quadratic index profile is designed based on the effective index of the first slab mode, the index profile of the higher-order modes can also be approximated by a quadratic profile; and (ii) since $\alpha' \approx \alpha$, the periodic distance for a higher mode is almost the same as that of the fundamental mode. Indeed, higher-order modes will propagate much faster compared with the fundamental mode. However, since the propagation distance within the waveguide is typically small, this should not be a concern as long as broad-bandwidth ultrashort pulses are not being used.

3. DESIGN EXAMPLES

Next we introduce and analyze specific design examples to further evaluate our novel waveguiding nanostructures. We evaluate the validity of these examples using FDTD analysis exploiting Rsoft's FullWAVE software package (Version 5.1). For the calculations we used a discrete grid with a cell size of 30×30 nm. The normalized time step was 21 nm. These values were chosen by reducing the grid size and observing the convergence of the optical field distribution.

Our first example aims to show that light can be focused within the slab by generating an effective graded-index profile by using a 1-D subwavelength structure configuration. To meet current fabrication constraints, the minimal feature size (i.e., postwidth) and the minimal air gap were chosen to be 100 nm. The period is 0.4 μm (smaller than the λ/n limit), and thus the duty ratio is allowed to vary between 25% and 75%. Assuming a slab effective index of 3.3 (corresponding to slab thickness of ~ 1 μm), the local effective index at $x = 0$ [see Eq. (1a)] is 3. We designed an effective index profile of $n_0 = 3.0$, $\alpha = 0.01$ $(1/\mu m^2)$ allowing an aperture of 16 μm along the x axis. The device length is 10 μm. On the basis of the Gaussian matrix approach [Eqs. (5)–(7)], a beam waist of 6.5 μm (full width) at the front end of the structure will be focused to a spot size of 1.37 μm at a distance of 7.8 μm away from the rear end of the structure (i.e., 17.8 μm from the origin). Although one might expect degraded performance due to the narrow beam width that is expected to propagate beyond the paraxial approximation, this should not be a major concern since it was already shown that a device with a quadratic index profile will generate a focal point even for cases in which the paraxial approximation is violated (although focal length is expected to be slightly shorter).[35] Figure 6(a) shows a FDTD simulation of the Gaussian beam propagation through the device, clearly demonstrating the focusing effect. The obtained focal plane was located at a distance of 7.0 μm away from the rear end of the structure, which is slightly shorter than that predicted by the paraxial equation. The normalized field distribution at the focal plane is shown in Fig. 6(b). The obtained beam width was ~ 1.2 μm (slightly smaller than the paraxial prediction). For comparison purposes, a Gaussian beam with a diameter of 1.2 μm is also plotted. The focused beam profile fits reasonably well with that of the Gaussian beam. The sidelobes observed in Fig. 6(b) are expected for nonparaxial Gaussian beam focusing.[35] The power carried by the focused beam is $\sim 95\%$ of the launched Gaussian beam. The loss is mainly due to reflection and scattering at the boundary between the structure and the uniform slab.

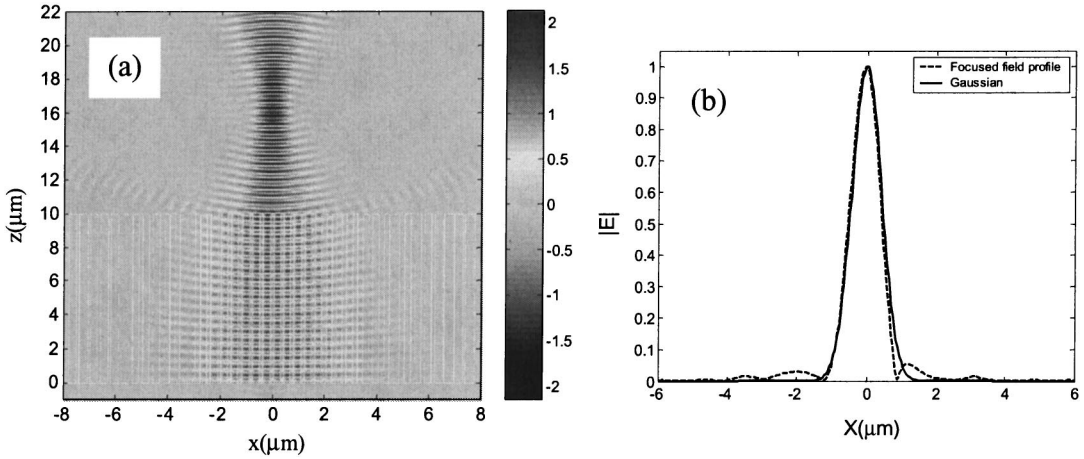

Fig. 6. Field propagation through a focusing graded-index lens with $n_0 = 3$, $\alpha = 0.01$ $(1/\mu m^2)$. The initial beam diameter is 6.5 μm. (a) Top view showing the focusing effect. (b) Cross section at the focus. For comparison purposes, the Gaussian beam profile is also displayed.

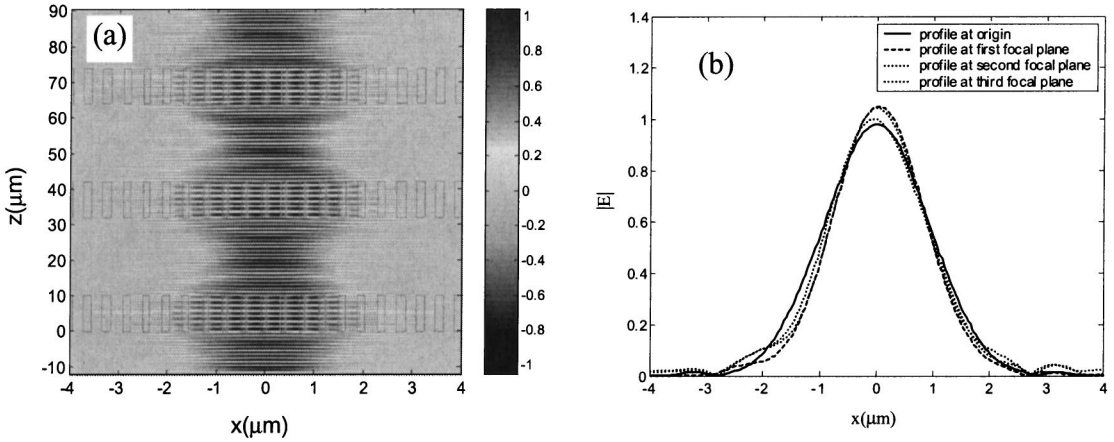

Fig. 7. Field propagation through a periodic subwavelength-based lens configuration. Each lens is similar to that shown in Fig. 6. The initial beam diameter is 2.5 μm.

The obtained results clearly show that subwavelength-based graded-index components behave as a lenslike media and that our approximate design concepts are reasonably valid. The beam waist can be controlled by the gradient of the effective index, as well as by the initial beam waist. Therefore such a device can be very useful for mode matching between waveguides with different dimensions. It can also assist the coupling from an optical fiber.

Next we combine several such lenses to achieve guiding-equivalent propagation by using a cascade of lenses, known in free-space systems as a lens waveguide or a relay-lens structure. The most simple configuration of such a relay-lens waveguide is designed with the beam waist located in the middle between two consecutive lenses. With this arrangement, the distance between two consecutive lenses (L) is usually chosen to be equivalent to twice the Rayleigh distance: $L = 2Z_0 = 2[(\pi\omega_0{}^2)/\lambda]n$, so that the beam spreads only by a factor of $\sqrt{2}$ compared to its width at the waist. For our simulation we assumed $\omega_0 = 1.25$ μm, leading to $L = 22$ μm. As a building block for the proposed configuration, we used our subwavelength-based graded-index medium with parameters equivalent to the lens presented above. The beam propagation through the proposed design was simulated with the FDTD method. The obtained results are shown in Fig. 7. Figure 7(a) shows a top view of the field propagation through the lens array. We observe that the beam is practically guided by the periodic lens cascade. For comparison, a Gaussian beam with similar parameters propagating through a uniform slab waveguide of similar length (96 μm) would expand by a factor of 9 compared with its original beam size. Figure 7(b) shows the beam profile at each focal plane. One can see that the beam profile repeats itself and fits the original Gaussian beam very well. The loss per stage is of the order of 1–2%, mainly due to reflection from the boundaries. Reflection losses can be further reduced by considering a tapered geometry, where the edges of the structure (along the z axis) are designed to have a triangular shape. With the proposed configuration the interaction length of the propagating light with the subwavelength structure is much smaller than the actual propagation distance, thus scattering losses are expected to be reduced (although the latter issue might be subject to dispute and needs to be further investigated). Cascading of several such lenses can also be useful for the implementation of miniaturized integrated optical signal processing systems performing on-chip correlations and transformations. For these latter applications issues such as space–bandwidth product and information capacity need to be further estimated.

So far, we have considered graded-index devices with a relatively short propagation length. Nevertheless, it is possible to fabricate much longer subwavelength-based graded-index components that can be used for the implementation of graded-index waveguides, where the optical guidance is provided by periodic focusing of the light propagating within the structure. In general, a graded-index waveguide is a multimode structure, and thus the beam size is not uniform along the propagation axis. Nevertheless, by proper choice of incident beam size, one can develop an interesting alternative for guiding through the supercollimation effect,[26,27] i.e., the beam size can be kept intact along the propagation axis. In contrast to the conventional supercollimation, where the beam size is maintained constant by the flattening of the dispersion curve, our supercollimated device is based on the balancing of the diffraction of the Gaussian beam and the focusing power of the subwavelength-based graded-index component for a specific beam waist. We assume that the launching conditions are such that the Gaussian beam waist is located at the front end of the structure. As a result, there is no phase curvature, i.e., $R \to \infty$. To achieve supercollimation-like behavior, we require $R \to \infty$ regardless of the z coordinate. This corresponds to the requirement that q_{out} is purely imaginary, i.e.,

$$\mathrm{Re}(q_{\text{out}}) = \mathrm{Re}\left(\frac{Aq_{\text{in}} + B}{Cq_{\text{in}} + D}\right) = 0, \tag{8}$$

where $q_{\text{in}} = -j[(\pi\omega_0{}^2 n)/\lambda]$.

With a few simple algebraic steps, the required beam half-width at the waist is found to be

$$\omega_0 = \left(\frac{\lambda}{n\pi\sqrt{\alpha}}\right)^{1/2}. \tag{9}$$

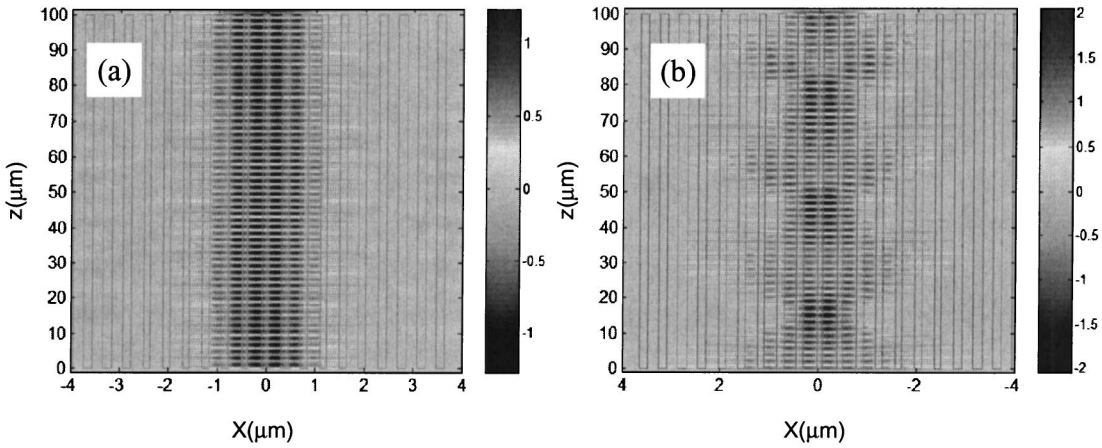

Fig. 8. Field propagation through a subwavelength-based graded-index waveguide with the effective index parameters $n_0 = 3$, $\alpha = 0.01\ (1/\mu m^2)$. The beam diameter at the front end of the structure was chosen to be (a) 2.4 μm, (b) 4.5 μm. In (a) a supercollimation characteristic is demonstrated since the diffraction and the focusing power are balanced.

For such a waist half-width, the diffraction and the focusing phenomena balance each other, and the Gaussian beam will maintain its horizontal dimension throughout the propagation within the nanostructure-based graded-index waveguide (equivalent to the propagation of a single horizontal mode). An FDTD simulation of a Gaussian beam propagating through a graded-index waveguide with $n_0 = 3$, $\alpha = 0.01\ (1/\mu m^2)$ is demonstrated in Fig. 8. For Fig. 8(a) the beam-waist half-width was chosen to be 1.2 μm, in accordance with Eq. (9) to achieve supercollimation characteristics. To contrast the supercollimation design, a beam-waist half-width of 2.25 μm is depicted in Fig. 8(b). We observe that the beam shown in Fig. 8(a) demonstrates nearly constant width as it propagates through the structure, whereas the beam width shown in Fig. 8(b) expands and contracts periodically, as usually occurs in a typical quadratic graded-index waveguide where multimode propagation occurs. These two examples clearly show that the beam can be guided along the chip, and its transverse dimensions can be manipulated by controlling the initial beam waist and the index gradient. The capability to control the beam width along the propagation axis is useful for applications involving coupling of light into functional devices on the chip as well as for efficient coupling of light into an output waveguide. Our 2-D simulation results show negligible propagation loss. However, for practical estimation of the propagation loss it would be best to conduct an experimental measurement. We intend to fabricate a device and to provide experimental results in the near future.

4. TECHNOLOGICAL CONSIDERATIONS

To estimate the feasibility of the proposed concept, fabrication constraints should be taken into account. To achieve high-performance devices, the fabrication procedure should provide accurate control over the duty ratio and the grating profile, uniform etching depth, smooth surfaces, and high aspect ratios. During recent years several authors demonstrated the fabrication of such high-quality structures with features on the 100-nm scale.[36–41] A typical fabrication process involves patterning the desired structure on a poly(methyl methacrylate)

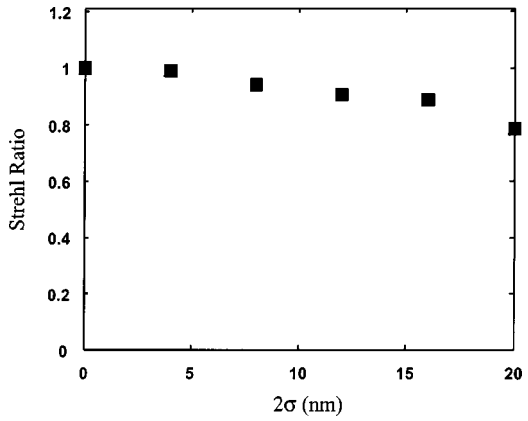

Fig. 9. Strehl ratio versus relative inaccuracy of the postwidth. Current technology supports an accuracy better than 10 nm, corresponding to a Strehl ratio larger than 0.9.

resist by use of electron-beam lithography, followed by pattern transfer into metal or SiO_2 mask. The mask pattern is then transferred to the substrate by use of reactive ion etching (RIE), reactive ion-beam etching (RIBE), or chemically assisted ion-beam etching (CAIBE). However, the accuracy of the fabricated structures can be limited.

Several authors describe a significant decrease in etching rate with the decrease of the air-gap width.[36,39,41–43] This phenomenon is known as reactive ion etching lag or microloading and can be overcome by use of an etching stop layer. For example, Ref. 36 demonstrates the usefulness of a 90-nm AlGaAs stop layer for the etching of variable-width gratings with uniform height in GaAs.

An additional concern is the limited accuracy of the postwidth. Although the absolute accuracy barely affects the index gradient, the relative accuracy of each post width is expected to have a significant effect on the device performance. To evaluate the effect of this fabrication inaccuracy, the original structure presented in Fig. 6 is perturbed by adding a normally distributed random number with a standard deviation of σ, where 2σ corresponds to the full width of the distribution. As a figure of merit for the quality of the perturbed lens, we use the Strehl ratio,

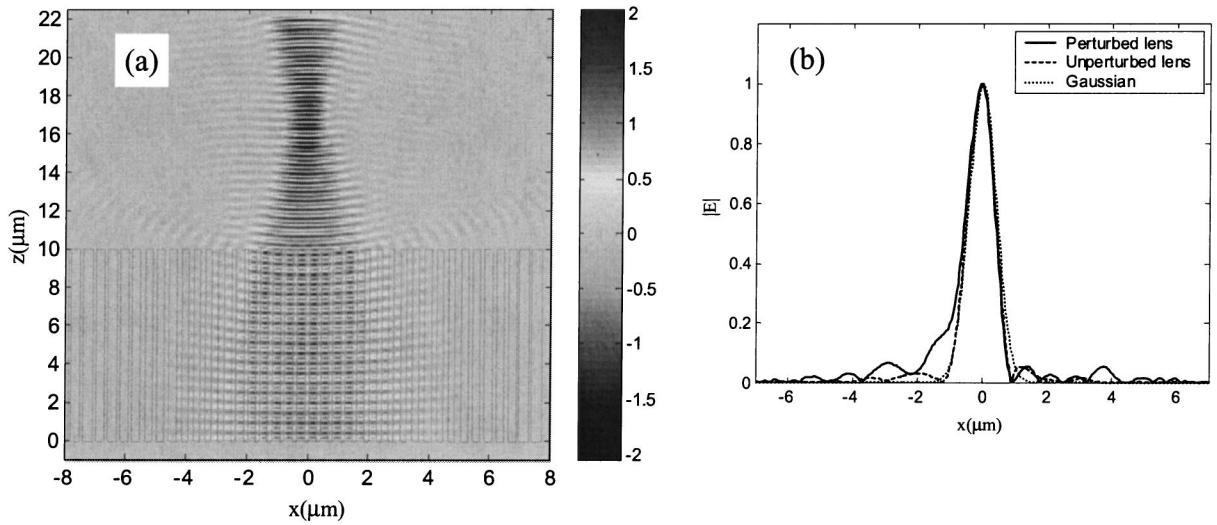

Fig. 10. Field propagation through the perturbed focusing graded-index lens with the same parameters as in Fig. 6. (a) Top view still showing a significant focusing effect. (b) Field profile at the focal plane. For comparison purposes, the unperturbed profile and a Gaussian beam profile are also displayed.

defined as $|\mathbf{E}_{\text{perturbed}}(x = 0, z = z_p)|^2/\mathbf{E}_{\text{unperturbed}}(x = 0, z = z_p)/^2$, where $\mathbf{E}_{\text{perturbed}}$ and $\mathbf{E}_{\text{unperturbed}}$ are the optical field distributions for the perturbed and the unperturbed lenses, respectively, and z_p is the distance of the focal plane from the origin. Figure 9 shows the expected Strehl ratio versus the fabrication accuracy limit (2σ). Each value was calculated by averaging the results ob tained from five different structures. To validate the accuracy of the FDTD calculation we reduced the horizontal cell size to 5 nm. The simulation results clearly show that the Strehl ratio decreases with the increase of the fabrication inaccuracies. To estimate the resolution accuracy that can be achieved with the current fabrication technology, we refer to Ref. 39, where the fabrication of an InP grating having a period of 390 nm and gap width varying from 90 to 290 nm in increments of 10 nm is described, and to Ref. 36 where the fabrication of a GaAs grating having a period of 330 nm and a postwidth varying from 50 to 180 nm in increments of ~20 nm is described. The results show that the fabrication of a grating with a postwidth accuracy better than 10 nm, an aspect ratio larger than 10, and smooth surfaces is feasible. This corresponds to a Strehl ratio better than 0.9 (see Fig. 9), which is considered to be sufficient for most applications. The properties of the perturbed lens having a width accuracy limit of 10 nm are depicted in Fig. 10. Figure 10(a) shows the Gaussian beam propagation through the perturbed device, clearly demonstrating a strong focusing effect. In Fig. 10(b) the beam profile at the focal plane is given. For comparison, the beam profile obtained with the unperturbed lens and a Gaussian profile are also displayed. This comparison shows only minor degradation of the beam profile obtained with the perturbed lens compared with that obtained with the unperturbed lens.

In view of these results, we believe that, although the realization of the proposed structures is challenging, the parameters used for our design examples in Section 3 are realistic and compatible with the current fabrication technology. With the progress in fabrication technology, the realization of these structures is expected to become less demanding.

5. CONCLUSIONS

We present and analyze a novel (to best of our knowledge) configuration for the implementation of graded-index devices based on subwavelength structures. The proposed concept is based on etching a 1-D periodic subwavelength structure with a varying duty ratio into a high-index slab waveguide. A quadratic effective index profile is achieved by modifying the duty ratio of the structure gradually along the horizontal axis, while the period is kept fixed. The beam is confined along the vertical axis by the slab waveguide, similar to 2-D photonic crystals. Novel configurations implementing graded-index lenses and waveguides are described, analyzed, and demonstrated numerically with an FDTD simulation tool. We also presented a design to obtain supercollimation beam propagation (i.e., the beam width is kept intact through the propagation within the nanostructure). This is achieved by proper choice of parameters, providing balance between the beam diffraction and the focusing power of the device. It was shown that guiding of light could also be achieved by cascading several such lenses along the propagation direction. The latter configuration offers a reduced interaction length of the propagation beam with the subwavelength structure and thus is expected to provide lower out-of-plane loss compared with the subwavelength-based waveguide. It should be noted that there are several percents of reflection loss at each interface between the components and the uniform slab. Reflection losses can be reduced by adiabatic modification of the structure along the z axis to achieve smooth index variations.

The proposed devices can be used for guiding, imaging, mode matching, coupling, and signal processing, while offering the intrinsic advantages of on-chip integration such as miniaturization, elimination of the need to align

each component separately, and manufacturability. They can also be integrated with other devices fabricated with such a material platform. On the basis of tolerance analysis, we believe that the realization of these novel devices is achievable with current fabrication technology.

ACKNOWLEDGMENTS

This work is supported in part by the U.S. Air Force Office of Scientific Research, the National Science Foundation, the Defense Advanced Research Projects Agency, and the Space and Naval Warfare Systems Command.

The e-mail address for U. Levy is ulevy@ece.ucsd.edu.

REFERENCES AND NOTES

1. I. Richter, P. C. Sun, F. Xu, and Y. Fainman, "Design considerations of form birefringent microstructures," Appl. Opt. **34**, 2421–2429 (1995).
2. F. Xu, R. Tyan, P. C. Sun, C. Cheng, A. Scherer, and Y. Fainman, "Fabrication, modeling, and characterization of form-birefringent nanostructures," Opt. Lett. **20**, 2457–2459 (1995).
3. R. Tyan, P. C. Sun, A. Scherer, and Y. Fainman, "Polarizing beam splitter based on the anisotropic spectral reflectivity characteristic of form-birefringent multilayer gratings," Opt. Lett. **21**, 761–763 (1996).
4. R. Tyan, A. Salvekar, Cheng, A. Scherer, F. Xu, P. C. Sun, and Y. Fainman, "Design, fabrication, and characterization of form-birefringent multilayer polarizing beam splitter," J. Opt. Soc. Am. A **14**, 1627–1636 (1997).
5. C. Gu and P. Yeh, "Form birefringence dispersion in periodic layered media," Opt. Lett. **21**, 504–506 (1996).
6. U. Levy and Y. Fainman, "Dispersion properties of inhomogeneous nanostructures," J. Opt. Soc. Am. A **21**, 881–889 (2004).
7. W. Nakagawa, R. Tyan, and Y. Fainman, "Analysis of enhanced second-harmonic generation in periodic nanostructures using modified rigorous coupled-wave analysis in the undepleted-pump approximation," J. Opt. Soc. Am. A **19**, 1919–1928 (2002).
8. D. L. Brundrett, E. N. Glytsis, and T. K. Gaylord, "Subwavelength transmission grating retarders for use at 10.6 μm," Appl. Opt. **35**, 6195–6202 (1996).
9. H. Kikuta, Y. Ohira, and K. Iwata, "Achromatic quarter-wave plates using the dispersion of form birefringence," Appl. Opt. **36**, 1566–1572 (1997).
10. G. Nordin and P. Deguzman, "Broadband form birefringent quarter-wave plate for the mid-infrared wavelength region," Opt. Express **5**, 163–168 (1999), www.opticsexpress.org.
11. F. T. Chen and H. G. Craighead, "Diffractive phase elements based on two-dimensional artificial dielectrics," Opt. Lett. **20**, 121–123 (1995).
12. J. N. Mait, A. Scherer, O. Dial, D. W. Prather, and X. Gao, "Diffractive lens fabricated with binary features less than 60 nm," Opt. Lett. **25**, 381–383 (2000).
13. D. W. Prather, J. Mait, M. S. Mirotzniki, and J. P. Collins, "Vector-based synthesis of finite aperiodic subwavelength diffractive optical elements," J. Opt. Soc. Am. A **15**, 1599–1607 (1998).
14. F. Xu, R. Tyan, P. C. Sun, Y. Fainman, C. Cheng, and A. Scherer, "Form-birefringent computer-generated holograms," Opt. Lett. **21**, 1513–1515 (1996).
15. U. Levy, C. H. Tsai, L. Pang, and Y. Fainman, "Engineering space-variant inhomogeneous media for polarization control," Opt. Lett. **29**, 1718–1720 (2004).
16. S. M. Rytov, "Electromagnetic properties of a finely stratified medium," Sov. Phys. JETP **2**, 466–475 (1956).
17. M. G. Moharam and T. K. Gaylord, "Rigorous coupled-wave analysis of planar grating diffraction," J. Opt. Soc. Am. **71**, 811–818 (1981).
18. A. Taflove and S. Hagness, *Computational Electrodynamics: The Finite-Difference Time-Domain Method*, 2nd ed. (Artech House, Norwood, Mass., 2000).
19. D. W. Parther, M. S. Mirotznik, and J. N. Mait, "Boundary integral methods applied to the analysis of diffractive optical elements," J. Opt. Soc. Am. A **14**, 34–43 (1997).
20. K. D. Paulsen, "Finite-element solution of Maxwell's equations with Helmholtz forms," J. Opt. Soc. Am. A **11**, 1434–1444 (1994).
21. D. Mendlovic, H. M. Ozaktas, and A. W. Lohmann, "Graded-index fibers, Wigner-distribution functions, and the fractional Fourier transform," Appl. Opt. **33**, 6188–6193 (1994).
22. J. D. Joannopoulos, R. D. Meade, and J. N. Winn, *Photonic Crystals* (Princeton U. Press, Princeton, N.J., 1995).
23. M. Loncar, D. Nedeljkovic, T. Doll, J. Vuckovic, A. Scherer, and T. P. Pearsall, "Waveguiding in planar photonic crystals," Appl. Phys. Lett. **77**, 1937–1939 (2000).
24. E. Chow, S. Y. Lin, S. G. Johnson, P. B. Villeneuve, J. D. Joannopoulos, J. R. Wendt, G. A. Vawter, W. Zubrzycki, H. Hou, and A. Alleman, "Three-dimensional control of light in a two-dimensional photonic crystal slab," Nature (London) **407**, 983–986 (2000).
25. H. Kosaka, T. Kawashima, A. Tomita, M. Notomi, T. Tamamura, T. Sato, and S. Kawakami, "Superprism phenomena in photonic crystals," Phys. Rev. B **58**, 10096–10099 (1998).
26. W. Lijun, M. Mazilu, and T. F. Krauss, "Beam steering in planar-photonic crystals: from superprism to supercollimator," J. Lightwave Technol. **21**, 561–566 (2003).
27. D. W. Prather, S. Shi, D. M. Pustai, C. Chen, S. Venkataraman, A. Sharkawy, G. J. Schneider, and J. Murakowski, "Dispersion-based optical routing in photonic crystals," Opt. Lett. **29**, 50–52 (2004).
28. O. Montalien, V. Brioude, A. Tishchenko, and O. M. Parriaux, "Optimization of the strength of a graded-index slab waveguide grating," in *Advances in Optical Thin Films*, C. Amra, N. Karsev, and H. A. Macleod, eds., Proc. SPIE **5250**, 609–618 (2004).
29. R. Magnusson and S. S. Wang, "New principle for optical filters," Appl. Phys. Lett. **61**, 1022–1024 (1992).
30. R. R. Boye and R. K. Kostuk, "Investigation of the effect of finite grating size on the performance of guided-mode resonance filters," Appl. Opt. **39**, 3649–3653 (2000).
31. P. Lalanne and D. L. Lalanne, "Depth dependence of the effective properties of subwavelength gratings," J. Opt. Soc. Am. A **14**, 450–458 (1997).
32. J. Canning, "Diffraction-free mode generation and propagation in optical waveguides," Opt. Commun. **207**, 35–39 (2002).
33. H. Kogelnik, "On the propagation of Gaussian beams of light through lenslike media including those with a loss and gain variation," Appl. Opt. **4**, 1562–1569 (1965).
34. We define the polarization with respect to the periodic structure, i.e., $\mathbf{E} = E\hat{y}$ for TE and $\mathbf{H} = H\hat{y}$ for TM. This is in opposition to the standard definition used in waveguide theory.
35. N. I. Petrov, "Focusing of beams into subwavelength area in an inhomogeneous medium," Opt. Express **9**, 658–673 (2001), www.opticsexpress.org.
36. C. Giaconia, R. Torrini, S. K. Murad, and C. D. W. Wilkinson, "Artificial dielectric optical structures: a challenge for nanofabrication," J. Vac. Sci. Technol. B **16**, 3903–3905 (1998).
37. W. J. Zubrzycki, G. A. Vawter, and J. R. Wendt, "High-aspect-ratio nanophotonic components fabricated by C12 reactive ion beam etching," J. Vac. Sci. Technol. B **17**, 2740–2744 (1999).
38. K. Avary, J. P. Reithmaier, F. Klopf, T. Happ, M. Kamp, and A. Forchel, "Deeply etched two-dimensional photonic crystals fabricated on GaAs/AlGaAs slab waveguides by using chemical assisted ion beam etching," Microelectron. Eng.

61–62, 875–880 (2002).
39. H. C. Kim, H. Kanjo, T. Hasegawa, S. Tamura, and Shigehisa Arai, "1.5-μm wavelength narrow stripe distributed reflector lasers for high-performance operation," IEEE J. Sel. Top. Quantum Electron. **9**, 1146–1152 (2003).
40. Z. Yu, L. Chen, W. Wu, H. Ge, and S. Y. Chou, "Fabrication of nanoscale gratings with reduced line edge roughness using nanoimprint lithography," J. Vac. Sci. Technol. B **21**, 2089–2092 (2003).
41. M. V. Kotlyar, L. O'Faolain, R. Wilson, and T. F. Krauss, "High-aspect-ratio chemically assisted ion beam etching for photonic crystals using a high beam voltage-current ratio," J. Vac. Sci. Technol. B **22**, 1788–1791 (2004).
42. D. Keil and E. Anderson, "Characterization of reactive ion etch lag scaling," J. Vac. Sci. Technol. B **19**, 2082–2088 (2001).
43. S. Panda, R. Ranade, and G. S. Mathad, "Etching high aspect ratio silicon trenches," J. Electrochem. Soc. **150**, G612–G616 (2003).